Forward Models can be Inferred from EEG Data

Submission Number:

1784

Submission Type:

Abstract Submission

Authors:

Sofie Therese Hansen[1], Søren Hauberg[1], Lars Kai Hansen[1]

Institutions:

[1]Technical University of Denmark, Kongens Lyngby, Denmark

Introduction:

Functional neuroimaging based on EEG is experimentally flexible and provides temporally detailed information of the ongoing brain activity. The activity is however spatially blurred by effects of volume conduction (Gevins 1999). These effects can be partly removed by solving the inverse problem of EEG (Besserve 2011), i.e. localizing the brain sources that create the activity the scalp electrodes measure.

Accurate source localization is contingent on an accurate forward model. The forward model maps the brain activation to electric potentials at the scalp. A successful mapping is reliant on detailed information of the head geometry and its electric properties (see e.g. Acar 2013). The conventional approach combines anatomical information from structural MR scans and assumed conductivities of the anatomical compartments.

We here propose an entirely data driven approach to forward model inference relieving the need for accurate anatomical information. Instead we build a low-dimensional parametrization of forward models using a corpus of subjects, see Fig.1. Using the EEG data of a new subject we optimize in this parametrization to infer both a subject-specific forward model *and* the sparse EEG source distribution.

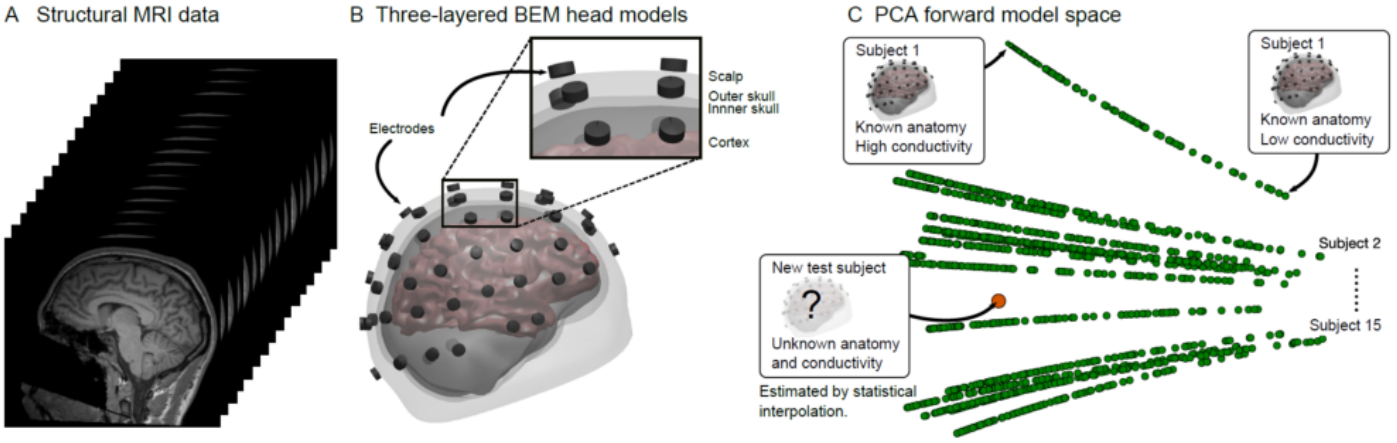

Figure 1: Parametrization of a corpus of forward models. The structural scans of the subjects (A) are segmented into scalp, skull and brain (B). For each subject 100 forward models are created with skull:brain conductivity ratios between 1:250 and 1:15. The forward models are projected into a 2D PCA space (C). Each horizontal line corresponds to one subject where brain conductivities of the forward models decrease from left to right. The forward model of a new subject can be inferred from this parametrization.

Methods:

A corpus of forward models is derived from MRI scans of 15 subjects from the multimodal neurimaging data set (Wakeman 2015), see Fig. 1A. The scans are segmented using SPM (Ashburner 2005) into three-layered boundary element method (BEM) head models consisting of scalp, skull and brain, see Fig. 1B. For each subject 100 forward models are constructed with skull:brain conductivity ratios between 1:250 and 1:15. Using principal component analysis (PCA) the 1500 forward models are projected into a 2D PCA space, see Fig 1C.

As PCA is a generative model a forward model for a new subject can be found within the space spanned by the training subjects. The optimal forward model is defined as having lowest free energy when combined with the new subject's EEG. The free energy is calculated during inference of the source activation by the Bayesian solver the Variational Garrote (VG) (Kappen 2011/2014, Hansen 2013), see Fig. 2.

The method is tested on a simulated and a real data set. The simulated EEG has 4 active sources across 25 time samples (Fig. 4D) and noise is added to yield an SNR of 5 dB. The real EEG data is the differential EEG response to seeing faces and scrambled faces of a subject participating in the applied multimodal data set.

$$\text{VG:} \quad Y_{kt} = \sum_{n=1}^{N} A_{kn} s_n X_{nt} + E_{nt}, \text{ where } E_{nt} \sim \mathcal{N}(0, 1/\beta) \text{ and } s_n \in \{0,1\} \tag{A}$$

$$\text{Posterior prob.:} \quad p(\mathbf{s}, \mathbf{X}, \beta | \mathbf{D}, \gamma) = \frac{p(\mathbf{X}, \beta) p(\mathbf{s}|\gamma) p(\mathbf{D}|\mathbf{s}, \mathbf{X}, \beta)}{p(\mathbf{D}|\gamma)}, \text{where } p(\mathbf{s}|\gamma) = \prod_{i=1}^{n} p(s_i|\gamma) \text{ and } p(s_i|\gamma) = \frac{\exp(\gamma s_i)}{1+\exp(\gamma)} \tag{B}$$

$$\text{Approximation:} \quad \log p(\mathbf{X}, \beta | \mathbf{D}, \gamma) \propto \log \sum_{\mathbf{s}} p(\mathbf{s}|\gamma) p(\mathbf{D}|\mathbf{s}, \mathbf{X}, \beta) \geq -\sum_{\mathbf{s}} q(\mathbf{s}) \log \frac{q(\mathbf{s})}{p(\mathbf{s}|\gamma) p(\mathbf{D}|\mathbf{s}, \mathbf{X}, \beta)} = -F \tag{C}$$

$$\begin{aligned} \text{Free energy:} \quad F(\mathbf{m}, \mathbf{X}, \beta, \mathbf{Z}, \lambda) = & -\frac{Tp}{2} \log \frac{\beta}{2\pi} + \frac{\beta}{2} \sum_{t=1}^{T} \sum_{k=1}^{K} (Z_{kt} - Y_{kt})^2 + \frac{K\beta}{2} \sum_{t=1}^{T} \sum_{n=1}^{N} m_n (1-m_n) X_{nt}^2 \chi_{nn} + N \log(1+\exp(\gamma)) \\ & - \gamma \sum_{n=1}^{N} m_i + \sum_{n=1}^{n} (m_n \log(m_n) + (1-m_n) \log(1-m_n)) + \sum_{t=1}^{T} \sum_{k=1}^{K} \lambda_{kt} \left(Z_{kt} - \sum_{n=1}^{N} m_n X_{nt} A_{kn} \right) \end{aligned} \tag{D}$$

Figure 2. (A) VG mapping of source n, X_{nt}, to electrode k, Y_{kt}, at time sample t through forward model $\mathbf{A}$. The binary variable s_n dictates whether source n is active or not. (B) Posterior probability of VG. The hyperparameter γ controls the degree of sparsity. (C) VG inference using the variational approximation $q(\mathbf{s})$, assuming flat prior on $\mathbf{X}$ and β and using Jensen's inequality. (D) Dual formulation of the free energy where $Z_{kt} = \sum_{n=1}^{N} m_n X_{nt} A_{kn}$, λ are lagrange multipliers and χ is the covariance matrix of $\mathbf{A}$.

Results:

The results of the simulation are summarized in Fig. 3 and clarified in Fig. 4A-D. The free energy computed for the EEG data of the new subject (withheld from PCA) is seen in Fig. 4A. Knowing the locations of the activation allows calculation of the localization error (Fig 4B) and the F-measure (Fig. 4C). We see that the forward model having lowest free energy also has perfect source reconstruction in terms of these measures. Furthermore the found forward model is seen to approximate the true source distribution (Fig. 4D).

The results of the method applied to the face-evoked EEG response are seen in Fig. 4E-F and are in Fig. 4G compared to using the subject's MRI and template conductivity ratio. The two estimated source activations are similar and both peak 160 ms after stimulus onset and are located in the vicinity of the fusiform/occipital face areas.

Forward models	(A) Predicted from free energy	(B) Template MRI, template $\sigma_{skull:brain}$	(C) Subject MRI, template $\sigma_{skull:brain}$	(D) Subject MRI, true $\sigma_{skull:brain}$
Free energy	2994	3192	3057	2956
F-measure*	1	0	0.44	0.5
Localization error**				
Left posterior	0 mm	16.7 mm	15.1 mm	0 mm
Right posterior	0 mm	18.4 mm	6.0 mm	6.0 mm
Left anterior	0 mm	19.7 mm	0 mm	5.7 mm
Right anterior	0 mm	23.7 mm	0 mm	0 mm
Sum	**0 mm**	**78.5 mm**	**21.1 mm**	**11.7 mm**

Figure 3: Performance of source localization on simulated data when using (A) the forward model with lowest free energy in the PCA space, (B) the forward model derived from a template MRI and the SPM template skull:brain conductivity ratio 1:80, (C) the forward model derived from the MRI scan of the subject and the template conductivity ratio and (D) the forward model derived from the subject's MRI scan and the conductivity ratio used in the simulation.

* $\text{F-measure} = 2\frac{\text{precision} \cdot \text{recall}}{\text{precision} + \text{recall}}$

** The localization error is calculated as the Euclidean distance between the true and planted activation in each half hemisphere.

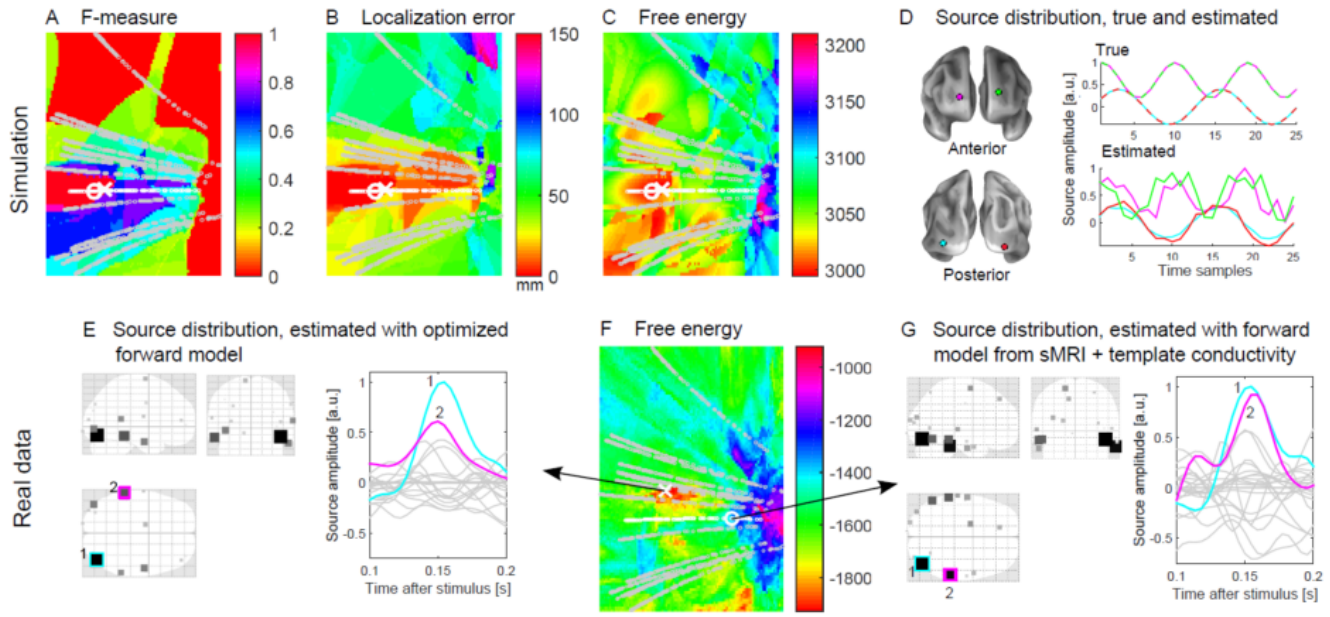

Figure 4: Validation using simulated data (top row) and the face-evoked EEG response (bottom row). (A) F-measure, (B) localization error and (C) free energy calculated for the simulated data. The forward model used in the simulation is indicated by a white circle and the free energy predicted forward model by a white 'X'. (D) The locations and temporal dynamics of the simulated sources (dashed lines) and the source activation estimated using the predicted forward model (full lines). Note that true and estimated locations are the same. (E) Source distribution for the real EEG data estimated using the predicted forward model, indicated in (F) by a white cross. (G) Source distribution estimated using a forward model derived from the subject's MRI and the template skull:brain conductivity ratio, 1:80. Location of this forward model corresponds to the white circle in (F). The forward models of the training subjects are indicated by small grey circles and the new subject's forward models (withheld from PCA) are shown as white small circles in (A)-(C) and (F).

Conclusions:

We have challenged the conventional approach to forward model inference, and shown that it is possible to infer both anatomical and conductivity aspects of a subject-specific forward model from EEG data. Our approach is data driven: We have introduced a low-dimensional parametrization of forward models based on a public collection of forward models. As open neuroimaging data bases expand data driven approaches will gain accuracy and in the specific case of forward modeling, the new approach may imply that we can increase the accuracy of EEG based neuroimaging.

Imaging Methods:

Anatomical MRI
EEG

Modeling and Analysis Methods:

Bayesian Modeling
EEG/MEG Modeling and Analysis [1]
Methods Development [2]

Keywords:

Data analysis
Electroencephaology (EEG)
Machine Learning
Modeling
MRI
Source Localization
STRUCTURAL MRI

[1|2]Indicates the priority used for review

Would you accept an oral presentation if your abstract is selected for an oral session?

Yes

I would be willing to discuss my abstract with members of the press should my abstract be marked newsworthy:

Yes

Please indicate below if your study was a "resting state" or "task-activation" study.

Task-activation

Healthy subjects only or patients (note that patient studies may also involve healthy subjects):

Healthy subjects

Internal Review Board (IRB) or Animal Use and Care Committee (AUCC) Approval. Please indicate approval below. Please note: Failure to have IRB or AUCC approval, if applicable will lead to automatic rejection of abstract.

Not applicable

Please indicate which methods were used in your research:

EEG/ERP
Structural MRI
Computational modeling

For human MRI, what field strength scanner do you use?

3.0T

Which processing packages did you use for your study?

SPM

Provide references in author date format

Gevins, A. (1999), 'Electroencephalographic imaging of higher brain function', Philosophical Transactions of the Royal Society of London, vol. 354, no. 1387, pp. 1125–1133.
Besserve, M. (2011). 'Improving quantification of functional networks with EEG inverse problem: evidence from a decoding point of view', NeuroImage, vol. 55, no. 4, pp. 1536–1547.
Akalin Acar, Z. (2013), 'Effects of forward model errors on EEG source localization', Brain Topography, vol. 26, no 3, pp. 378–396.
Kappen, H.J. (2011), 'The Variational Garrote', arXiv preprint, arXiv:1109.0486.
Kappen, H.J. (2014), 'The Variational Garrote', Machine Learning, vol. 96, no. 6, pp. 269-294.
Hansen, S.T. (2013), 'Sparse Source EEG Imaging with the Variational Garrote', 3rd International Workshop on Pattern Recognition in Neuroimaging (PRNI), pp. 106-109.
Wakeman, D. G. (2015). 'A multi-subject, multi-modal human neuroimaging dataset', Scientific Data, vol. 2, no. 150001.